Research Square

Preprints are preliminary reports that have not undergone peer review.
They should not be considered conclusive, used to inform clinical practice,
or referenced by the media as validated information.

Infection and injury cooperatively induce a tissue resident adaptive NK cell program that propagates lung damage and mortality

Daniel Calabrese

daniel.calabrese@ucsf.edu

University of California, San Francisco https://orcid.org/0000-0002-0596-3434

Reena Bharti

, Regional Centre for Biotechnology, National Capital Region Biotechnology Science Cluster,

Natalie Mosqueda

UCSF https://orcid.org/0000-0002-3860-6759

Dongliang Zhang

UCSF https://orcid.org/0009-0003-2500-1341

Longhui Qiu

University of California, San Francisco

Francesca Lunardi

University of Pavia

Annika Schmidt

UCSF https://orcid.org/0009-0007-6080-1677

Avishai Shemesh

UCSF https://orcid.org/0000-0002-6934-7155

Jonathan Singer

University of California, San Francisco

Steven Hays

University of California, San Francisco

Oscar Aguilar

UCSF https://orcid.org/0000-0002-7990-8745

Mark Looney

University of California San Francisco https://orcid.org/0000-0003-0241-9190

John Greenland

University of California, San Francisco https://orcid.org/0000-0003-1422-8367

Article

Keywords: Cytomegalovirus, acute lung injury, primary graft dysfunction, lung transplantation

Posted Date: October 26th, 2026

DOI: https://doi.org/10.21203/rs.3.rs-10686332/v1

License: This work is licensed under a Creative Commons Attribution 4.0 International License.
Read Full License

Additional Declarations: Yes there is potential Competing Interest. D.R.C. receives investigator-initiated grant support from Kamada and investigator-initiated research support from Natera, serves on an advisory board for Incyte, and previously received investigator-initiated grant support from DrenBio. DrenBio develops antibodies targeting CD94, and Kamada develops therapies in the cytomegalovirus field. None of these entities had any role in the conceptualization, design, data collection, analysis, decision to publish, or preparation of this manuscript. The remaining authors declare no competing interests.

Abstract

Cytomegalovirus (CMV) is a herpesvirus that persists latently after acute infection and reactivates during periods of stress. CMV infection remains a major driver of morbidity in solid organ transplant recipients, and how it worsens transplant outcomes is unknown. In 669 lung transplant recipients, latent donor CMV and primary graft dysfunction (PGD), a severe form of acute lung injury, synergistically promoted CMV reactivation, worse gas exchange, and mortality. In mice, ischemia-reperfusion injury reactivated latent CMV and drove durable expansion of tissue-resident, adaptive-like natural killer (NK) cells. Adoptive transfer of CMV-educated Ly49H$^+$ NK cells was sufficient to induce acute lung injury. Mortality tracked this NK cell program rather than viral load. Depleting NK cells prevented injury and rescued survival, whereas suppressing viral replication with ganciclovir did not. While CMV clinical trials to date have targeted suppression of viral replication, these findings reframe CMV-associated injury as an NK cell-driven process and identify the local adaptive NK compartment as a tractable therapeutic target.

Introduction

Cytomegalovirus (CMV) is a herpesvirus that persists latently for the life of the host after acute infection, reaching a seroprevalence above 90% in some populations [1]. The lung is a major site of CMV infection and a principal reservoir for latency in humans in concert with the salivary gland in mice [2]. In lung transplantation, CMV is a major determinant of long-term outcomes. Despite antiviral prophylaxis, over 40% of recipients develop CMV reactivation, which doubles the risk of graft failure [3]. Whether this injury is driven by viral replication itself or by the host immune response that CMV provokes remains unresolved. This is a distinction with direct therapeutic consequences as CMV durably reshapes immune phenotype and function, producing heterologous immunity and immune dysregulation that persists beyond the initial infection [4–6].

Prior work suggests the host immune response is a key component driving the association between CMV and poor clinical outcomes in transplantation. Natural killer (NK) cells are innate lymphocytes that survey tissue for missing-self, infected, or stressed cells through germline-encoded activating and inhibitory receptors [7,8] that engage ligands on target cells [9]. They restrain CMV through direct and antibody-dependent cytotoxicity while shaping T cell [10] and B cell immunity through interferon-γ [11]. In humans, the activating receptor NKG2C identifies a CMV-specific NK cell population [12] that undergoes avidity selection and persists as long-lived, adaptive-like memory cells [13]. In mice, an analogous virus-specific, memory-like NK response is well described via the Ly49H receptor that recognizes m157 – a virally encoded ligand [14–16]. In a longitudinal cohort of lung allograft recipients, expansion of NKG2C + NK cells in the bronchoalveolar lavage preceded CMV viremia, and higher NKG2C + NK cell frequencies conferred increased risk for chronic rejection and death, implicating CMV-specific tissue NK cells, rather than the virus alone, as potential mediators of allograft injury [17,18].

How injury might engage these adaptive NK cells is unknown. Acute lung injury (ALI), defined by alveolar-capillary barrier disruption, inflammatory cell infiltration, and impaired gas exchange, is the shared pathobiological endpoint of several clinically important conditions including primary graft dysfunction (PGD), ischemia-reperfusion injury, bacterial pneumonia, and sepsis[19–22]. In the first 72 hours after lung transplant, roughly 30% of recipients develop PGD, a form of acute lung injury driven by ischemia-reperfusion injury (IRI) [23]. PGD accounts for approximately half of first-year mortality after lung transplant and has no specific therapy [24]. It shares its defining physiology, impaired oxygenation and bilateral pulmonary opacities [25], with the acute respiratory distress syndrome (ARDS), the most severe form of acute lung injury [20,26], which causes more than 190,000 cases annually in the United States and carries over 40% mortality [27]. Both are marked by endothelial and epithelial dysfunction, inflammatory mediator release, and innate and adaptive immune activation [24,28–30]. We have shown that NK cells directly contribute to this injury: NK cells activated through the stress-ligand receptor NKG2D drive lung IRI and worsen PGD severity and transplant outcomes, and NK cells likewise promote endotoxin-induced lung injury as a model of ARDS [31–33]. Because acute organ injury is itself a trigger for CMV reactivation [34–36], we reasoned that injury-induced ligands could co-engage NKG2D and the CMV-specific receptor, both activating receptors that signal through the NKG2C-associated DAP10 in humans or NKG2D-associated adaptor [37,38], to amplify local NK cell activation and lung damage. Here, we tested the hypothesis that acute lung injury amplifies the local adaptive NK cell response to CMV, and that this virus-specific response, rather than viral replication alone, drives worse lung physiology and outcomes.

Results

Acute lung injury reactivates latent pulmonary cytomegalovirus

We examined the relationship between donor CMV serostatus, severe PGD, and early CMV reactivation in a cohort of 669 lung transplant recipients. Baseline characteristics are shown in Table 1 with inclusion criteria displayed in **Supplemental Fig. 1**. Of the 669 recipients, 77 developed CMV DNAemia during the follow-up period. Strikingly, we found that cumulative incidence of CMV DNAemia over the first 2 post-transplant years was highest among recipients with latent donor CMV and severe PGD, conferring a nearly 2-fold increased risk relative to other groups (hazard ratio [HR] 1.87, 95% confidence interval [CI] 1.11–3.17, adjusted p = 0.02, Fig. 1A). Risk of CMV DNAemia was also elevated in recipients with latent donor CMV alone.

Table 1
Cohort characteristics (N = 669)

characteristic	overall
	N = 669
Age, median [IQR]	61.00 [52.00, 66.00]
Male sex, N (%)	379 (56.7)
Ethnicity, N (%)	
White	423 (63.2)
Black	49 (7.3)
Hispanic	126 (18.8)
Asian	52 (7.8)
Other	19 (2.8)
Double lung transplant, N (%)	593 (88.6)
Transplant indication, N (%)	
COPD	100 (15.0)
pHTN	24 (3.6)
CF/Bronchiectasis	43 (6.4)
ILD	501 (75.0)
CMV serostatus, N (%)	
R−/D−	98 (14.6)
R−/D+	160 (23.9)
R+/D−	130 (19.4)
R+/D+	252 (37.7)
Unknown	28 (4.2)
Unknown/D+	1 (0.1)
Severe PGD, N (%)	156 (23.3)

Abbreviations: CF, cystic fibrosis; CMV, cytomegalovirus; COPD, chronic obstructive pulmonary disease; D, donor CMV IgG serostatus; ILD, interstitial lung disease; IQR, interquartile range; PGD, primary graft dysfunction; pHTN, pulmonary hypertension; R, recipient CMV IgG serostatus.

As higher circulating CMV copies have been associated with mortality [39], we further hypothesized that severe PGD would induce a more severe CMV reactivation profile. The distribution of first-year CMV DNAemia severity grades across the four groups is shown in Fig. 1B. Recipients with latent donor CMV and severe PGD had higher cumulative odds of increased CMV copies compared to the donor CMV negative and no PGD reference group (odds ratio [OR] 1.68, 95% CI 1.04–2.72, adjusted p = 0.03). Recipients with latent donor CMV and no PGD had intermediate risk (OR 1.40, 95% CI 0.97–2.02, p = 0.07), while severe PGD in the absence of donor CMV seropositivity was not associated with worse reactivation severity (OR 0.54, 95% CI 0.25–1.18, p = 0.12). The absence of an independent effect of PGD alone argues against a non-specific inflammatory mechanism and instead points to reactivation of a donor viral reservoir.

To investigate the mechanistic basis for these clinical observations, we generated a novel mouse model to test CMV reactivation from lung injury. We first characterized the kinetics of primary mouse CMV (mCMV) infection in C57BL/6 mice (Fig. 1C), demonstrating an expected rise-and-fall pattern of viral replication with establishment of latency before 60 post-infection days in all solid organs (Fig. 1D). mCMV IE-1 expression declined to below the limit of detection in both blood and lung by approximately 50 days post-infection, consistent with establishment of latency (Fig. 1E). We then asked whether lung ischemia-reperfusion injury (IRI), an established model of severe PGD, was sufficient to trigger reactivation from latency (Fig. 1F). We found lung IRI induced rapid reactivation of mCMV in the blood (Fig. 1G) and in the lung (Fig. 1H, p = 0.02) compared to sham procedures.

To understand if this mCMV reactivation phenomenon was specific to IRI alone, we performed analogous experiments using intratracheal lipopolysaccharide (LPS) to induce ALI (**Supplemental Fig. 2A**). Indeed, endotoxin acute lung injury (ALI) induced CMV DNAemia (**Supplemental Fig. 2B**) and lung CMV reactivation (**Supplemental Fig. 2C, p** = 0.02) relative to intratracheal saline control. These data demonstrate that ALI, both from IRI or endotoxin exposure, is sufficient to trigger CMV reactivation from latency *in vivo*, providing a plausible mechanistic explanation for the synergistic relationship between severe PGD and donor CMV serostatus observed in the clinical cohort.

Latent pulmonary cytomegalovirus amplifies the severity of acute lung injury

To determine whether latent donor CMV (DCMV+) influences the severity of ALI after transplantation, we examined PGD severity on postoperative day 3 (POD3) in the clinical cohort, stratified by donor CMV serostatus and severe PGD. Using ordinal logistic regression, we found that severe PGD in the setting of latent donor CMV (PGD+/DCMV+) conferred higher odds of more severe injury by the ratio of arterial oxygen (PaO_2) to the fraction of inspired oxygen (FiO_2, P:F), relative to the PGD−/DCMV− reference (adjusted OR 4.42, 95% CI 2.19–8.92, p < 0.0001; Fig. 2A). Severe PGD without donor CMV was also associated with worse grade of P:F (p = 0.001), whereas donor CMV positivity alone, in the absence of severe PGD, conferred no increased risk (p = 0.98). The compounding effect of donor CMV and severe

PGD was most apparent in ventilator mechanics. Compared to the no PGD and no latent donor CMV group, the PGD+/DCMV+ group exhibited the highest POD3 plateau pressure ($p < 0.001$, Fig. 2B), and the highest driving pressure (ΔP) ($p = 0.02$; Fig. 2C). By contrast, severe PGD in donor CMV-seronegative lungs showed a blunted increase in plateau pressure and no effect on driving pressure indicating that latent donor CMV accentuated the mechanical derangement of severe PGD.

To test whether latent CMV causes worsened ALI, we used the mouse model of latent mCMV with IRI or sham surgery performed during CMV latency (Fig. 2D). Latent CMV combined with IRI produced the most severe injury across all readouts. Arterial PaO_2 was lowest in the latent CMV/IRI group, significantly below mock/sham ($p < 0.0001$), latent CMV/sham ($p < 0.0001$), and mock/IRI ($p = 0.0005$), indicating that latent CMV worsened arterial oxygen beyond IRI alone (Fig. 2E). Total BAL protein, a marker of alveolar-capillary permeability, was correspondingly highest in the latent CMV/IRI group compared to mock/sham ($p = 0.002$), latent CMV/sham ($p = 0.005$), and mock/IRI ($p = 0.02$; Fig. 2F). Representative histological sections recapitulated these findings, with the latent CMV/IRI group showing the most severe parenchymal injury, characterized by extensive alveolar edema, marked septal thickening, and disruption of the normal alveolar architecture (Fig. 2G). These qualitative observations were corroborated by blinded histological scoring, which demonstrated significantly greater lung injury in the latent CMV/IRI group than in the latent CMV/sham group ($p = 0.004$), whereas no significant differences were observed between the mock groups (Fig. 2H). Finally, we confirmed these findings in a separate model of endotoxin induced lung injury (**Supplemental Fig. 2D & 2E**). Collectively, the clinical and experimental findings provide converging evidence that latent CMV amplifies ALI, exacerbating the severity of both PGD, IRI, and endotoxin-induced lung injury.

Latent CMV reactivation after IRI drives expansion and adaptive differentiation of lung NK cells

We hypothesized that IRI in the setting of latent CMV infection would drive a lung-specific adaptive NK cell immune response. To assess NK cells longitudinally, we used the same CMV latency model and collected lungs for phenotyping (Fig. 3A, n = 5–6 mice per group) at 6 hours and 60 days following IRI or sham in mock or CMV latently infected mice. Gating strategies are shown in **Supplemental Figs. 3A, 3B & 3C**.

IRI alone produced a transient rise in total NK cells: in mock-infected animals, NK frequency and number increased at 6 hours compared to sham as a percentage of lymphocytes (adjusted $p = 0.02$, Fig. 3B) and in total counts ($p = 0.02$, Fig. 3C) but no longer differed from sham at 60 days following IRI. In contrast, latent CMV combined with IRI produced a markedly larger and durable expansion. NK cells rose from a median of 7.7% to 24.8% of lymphocytes at 6 hours ($p = 0.04$) and from 5.8% to 25.5% of lymphocytes at 60 days ($p = 0.02$), with total counts increasing between 20- to 30-fold over latent CMV/sham at both timepoints (6 h, $p = 0.02$; 60 days, $p = 0.05$). The NK cell expansion in latent CMV IRI lungs was

disproportionately composed of CMV-specific Ly49H$^+$ NK cells (Fig. 3D), at both 6 hours and 60 days after injury quantified as a percentage of total NK cells (Fig. 3E) and total Ly49H$^+$ NK cells (Fig. 3F).

The pre-adaptive (KLRG1$^-$Ly6C$^+$) and adaptive Ly49H$^+$ subsets (KLRG1$^+$Ly6C$^+$, Fig. 3G) reproduced this pattern. In total numbers, the pre-adaptive NK cell populations were increased in IRI/latent CMV lungs relative to sham/IRI lungs at 6 hours ($p = 0.02$, Fig. 3H) and 60 days ($p = 0.02$). Strikingly, adaptive NK cells were expanded relative to sham/latent CMV lungs at 6 hours ($p = 0.02$, Fig. 3I), with a persistently robust increase in the IRI/latent CMV group through 60 days ($p = 0.04$). Thus, latent CMV with IRI, but not either alone, were required to recruit, expand, and retain long-lived adaptive NK cells in the injured lung. For additional mechanistic validation, these findings were also mirrored in an endotoxin-induced model of acute lung injury (**Supplemental Fig. 2F & 2G**).

Within the IRI/latent CMV group, most adaptive NK cells express Ly49CI (Fig. 3J). The dominance and stability of the Ly49CI+ fraction over 60 days suggests clonal or semi-clonal selection during the adaptive NK cell response to CMV reactivation, with potential for enhanced effector functions. Similarly, within the IRI/latent CMV group, adaptive NK cells retained high and stable expression of tissue residency markers (CD49a, Fig. 3K; CD69, Fig. 3L), activation markers (NKG2D, Fig. 3M; DNAM1+, Fig. 3N) and evidence of degranulation (CD107a, Fig. 3O). These findings indicate that the adaptive program established early after reactivation persists, even as the surface differentiation and receptor repertoire of the population continues to evolve.

Synergy between IRI and CMV was less apparent in non-NK cell lymphocyte populations

In the acute phase, IRI rather than latent CMV drove immune cell changes. B cells were unchanged in frequency (**Supplemental Fig. 4A**) and number (**Supplemental Fig. 4B**). Macrophages were decreased as proportion of live leukocytes 6 hours after IRI in mock-infected lungs ($p < 0.05$, **Supplemental Fig. 4C**), without a significant change in total count (**Supplemental Fig. 4D**). T cells and CD4 T cells expanded after IRI in frequency (**Supplemental Fig. 4E & 4G**) and number (**Supplemental Fig. 4F & 4H**). These were general early injury responses, not specific to latent CMV.

CD8 and γδ T cells expanded acutely after IRI (**Supplemental Fig. 5A-G**), but CMV-associated memory inflation was injury-independent. In mock-infected lungs, CD8 T cells were increased 6 hours after IRI compared to sham in frequency (**Supplemental Fig. 5B, p** = 0.05) and total count (**Supplemental Fig. 5C, p** = 0.04). CD8 effector memory composition shifted with IRI in mock infected lungs (χ^2 $p < 0.0001$) but notably expanded as a function of time after CMV infection rather than from IRI (**Supplemental Fig. 5D**). γδ T cells likewise increased in frequency **(Supplemental Fig. 5E**) and number (**Supplemental Fig. 5F**) after IRI, most strikingly acutely in the CMV IRI group ($p = 0.01$). While there were differences in effector memory phenotypes between groups, γδ T cell memory did not notably expand with CMV over time (**Supplemental Fig. 5G**). Thus, as opposed to NK cells, where injury in latent CMV infection provoked a long-term adaptive NK cell response, T cell responses did not reflect an interaction between IRI or CMV.

Lung transplant recipient bronchoalveolar lavage adaptive NK cells display a tissue-resident, cytotoxic program and signal reciprocally with airway epithelium

To characterize the human NK cells positioned to respond to CMV and allograft injury, we analyzed NK cells from recipient BAL by single-cell RNA sequencing, as previously described [40]. Clustering within the NK cell population identified several biologically distinct subsets, including pre-adaptive and adaptive populations distinguished by *KLRC2* (NKG2C) and *B3GAT1* (CD57) expression and by loss of *FCER1G*, *SH2D1B*, and *ZBTB16*, the canonical signature of adaptive NK differentiation (Fig. 4A)[41].

Differential expression between adaptive and pre-adaptive NK cells compared to the remaining NK cells showed upregulation of the tissue-residency factor *ZNF683* (Hobit), the transcription factor *IKZF3*, the chemokines *CCL4* and *CCL5*, and effector genes including *GZMA*, *GZMK*, and *IFNG* (**Supplemental Fig. 6A**). Gene set enrichment defined the breadth of this program (Fig. 4B, **Supplemental Table 1**). Adaptive/pre-adaptive NK cells were enriched for cytotoxicity, chemokine trafficking, activating receptors, tissue residency, and the hallmark allograft rejection and TNFα/NF-κB pathways. There was relative downregulation of IFN-α, IFN-γ, IL-2/STAT5, and oxidative phosphorylation signaling. Notably, adaptive and pre-adaptive NK cells were strikingly positive for tissue residency transcripts and downregulated genes associated with egress (**Supplemental Fig. 6B**). Together these define a differentiated, tissue-resident NK cell population with a cytotoxic effector profile and a transcriptional signature overlapping that of allograft rejection.

To determine how these NK cells interact with airway epithelium, we merged these data with another previously described lung transplant airway epithelial cell cohort to infer cell-cell signaling [42]. Outgoing signaling from adaptive NK cells (Fig. 4C, **Supplemental Fig. 7**) was broad, comprising cytotoxic and inflammatory mediators (*GZMA, FASLG, IFNG, TNF*, lymphotoxin, and *LIGHT*) and the pro-fibrotic and repair mediators *TGFB1*, amphiregulin (*AREG*), and fibronectin (*FN1*) directed at epithelial targets. Adaptive NK cells also received signals from epithelium through multiple axes (Fig. 4D, **Supplemental Fig. 8**), including collagen- and laminin-integrin interactions, HLA-E engagement of the NKG2A and NKG2C receptors (KLRC1, KLRC2), MIF, and the NKG2D ligands MICA and RAET1E (ULBP4) with ciliated and secretory subsets as the principal ligand sources. Together, these data identify a tissue-resident adaptive NK population in the lung allograft with a cytotoxic, rejection-associated transcriptional program, situated at the airway epithelial interface and engaged in reciprocal signaling with epithelium through adhesion, stress-ligand, cytotoxic, inflammatory, and pro-fibrotic pathways.

Adaptive NK cells establish residency in collagen-enriched areas, and co-localize with T cells via CCR5 signaling

Given the findings in human BAL, we hypothesized that mouse NK cells in IRI/latent CMV lungs would localize to epithelium and adopt tissue residency spatial characteristics. We performed spatial profiling of sham latent CMV lungs at 6 hours (n = 1) and 60 days (n = 2), and in IRI latent CMV lungs at the same timepoints (n = 2, each). Cell attributions within the spatially profiled tissues are shown in **Supplemental**

Fig. 9. NK cells were a rare spatial population (< 1% of bins in all sections) whose representation rose with injury at both timepoints, paralleled by early increases in T cells and neutrophils (Fig. 5A & 5B). NK cell bins were spatially aggregated rather than dispersed, noted by NK-to-NK cell density enriched up to 3.9-fold over a permuted null and nearest-neighbor distances fell well below random in every section. Within the parenchyma, NK cells localized closest to alveolar epithelium (AT2, AT1) and endothelium and farthest from B-cell zones, and these distances contracted under IRI at 6 hours, indicating injury-associated condensation of the NK compartment toward epithelial and vascular niches (Fig. 5C, **Supplemental Fig. 10A**).

When profiling the ligand content of the NK neighborhood, the signals most consistently enriched near NK cells across sections were *Gzma* (mean proximity enrichment 2.1, p = 0.01), consistent with NK cell and lymphoid co-aggregation and *Ccl5* (enrichment 3, p = 0.001). At 60 days after IRI in latent CMV, the NK cell niche shifted towards collagen matrix relative to sham lungs, with higher proximity enrichment for *Gzma*, *Col4a1*, *Icam1*, *Col3a1*, *Tgfb1*, and *Nectin3* (Fig. 5D & **Supplemental Fig. 10B**). Overall, NK cells were enriched in IRI/latent CMV lungs in regions expressing collagen gene transcripts at 60 days (enrichment 1.1, permutation p = 0.01). Figure 5E shows NK cell bins distributed within Col4a1-high regions of the injured lung relative to sham. Hallmark-program analysis showed the NK cell niche was significantly enriched for IFNg -response (permutation p = 0.002) and allograft-rejection signatures 60 days after IRI (p = 0.008). By contrast, NKG2D-ligand and CXCR3-ligand proximity to NK cells were not significant in any condition, and several NK-relevant gene sets (FASLG, IFNg, type I IFN, IL-15/IL-18/IL-12, PD-L1) were too sparse to test. These findings provide an *in vivo* spatial correlate of the human BAL data, positioning NK cells within injured epithelial and collagen-rich niches marked by Ccl5 and rejection-associated programs, and anchoring the tissue-resident, cytotoxic adaptive NK phenotype to the airway epithelial interface where reciprocal NK cell–epithelial signaling occurs.

Ly49H + NK cells are sufficient for acute lung injury propagation

To test whether the CMV-educated, adaptive Ly49H$^+$ NK subset is sufficient to drive ALI, we sorted Ly49H$^+$ or Ly49H$^-$ NK cells from latently CMV-infected donors at day 65 post-infection and adoptively transferred them into *Il2rg*$^{-/-}$*Rag2*$^{-/-}$ recipients, which lack endogenous T, B, and NK cells. After reconstitution, mice were exposed to intratracheal LPS to induce ALI (Fig. 6A). The two transfer groups reconstituted the NK cell compartment, by total cell count, to a comparable extent (Fig. 6B, p = 1). Mice receiving Ly49H$^+$ NK cells had more in total count (Fig. 6C) and as a percentage of total NK cells (Fig. 6D) relative to the no transfer and Ly49H$^-$ groups. Despite comparable reconstitution, recipients of Ly49H$^+$ NK cells developed markedly worse lung injury. Arterial oxygenation (PaO_2) was significantly reduced in Ly49H$^+$ recipients compared to Ly49H$^-$ NK cell recipients (p = 0.03) or no-transfer controls (p = 0.007, Fig. 6E). In parallel, BAL total protein was increased in Ly49H$^+$ NK cell recipients relative to both Ly49H$^-$ NK cell recipients (p = 0.04) and no-transfer controls (p = 0.05, Fig. 6F). Transfer of Ly49H$^-$ NK cells did not yield worse lung injury relative to the no transfer group, indicating that the capacity to

amplify ALI is a function of the Ly49H⁺ adaptive subset. Together, these data demonstrate that CMV-educated, Ly49H⁺ NK cells carry enhanced injurious potential and are sufficient to drive ALI.

Latent CMV is associated with NK cell–dependent mortality after lung injury in humans and mice

We next asked whether latent CMV worsens survival after lung injury in humans and mice. In our human lung transplant cohort, we modeled the cumulative hazards for CLAD and death across the four combinations of PGD and donor CMV serostatus. In a covariate-adjusted, multistate Cox model, recipients with both PGD and a CMV-seropositive donor allografts had a 3.7-fold higher hazard of death than the PGD−/donor CMV− reference group (HR 3.66, 95% CI 2.02–6.64, $p < 0.001$), and donor CMV positivity in the absence of PGD also increased mortality (HR 1.76, 95% CI 1.05–2.93, $p = 0.03$), whereas PGD without donor CMV did not (HR 1.52, $p = 0.38$, Fig. 7A). Although the cumulative hazard for CLAD was modestly higher in PGD+ recipients, and highest in the PGD+/donor CMV− group, no PGD and donor-CMV combination was associated with CLAD in the adjusted model. Thus, PGD in the setting of donor CMV selectively increased the risk of death rather than CLAD.

To test causality of the human observations, we subjected latently CMV-infected mice to lung IRI, administering anti-NK1.1, ganciclovir, or vehicle before injury (Fig. 7B). Relative to vehicle-treated mice, NK cell-depleted mice and ganciclovir-treated mice had suppressed CMV DNAemia (**Supplemental Fig. 11A & 11B**). However, ganciclovir (n = 9) did not reduce the severity of acute injury relative to NK cell depletion (n = 7, Fig. 7C). In overall survival, latent CMV-infected mice receiving vehicle prior to IRI (n = 11) had the highest risk for death along with the ganciclovir-treated (n = 6) group, while no mortalities occurred in mock-infected (n = 5) and NK cell depletion (n = 6) mice (Fig. 7D, log-rank $p = 0.04$). Together, these data suggest that excess mortality is driven by the CMV-induced immune program rather than by active viral replication, consistent with the sufficiency of adaptive Ly49H⁺ NK cells to worsen injury in Fig. 6.

NK cell depletion resets the adaptive pulmonary niche

We hypothesized that NK cell depletion and ganciclovir therapies would alter the CMV-associated adaptive NK cell population that accumulates in the injured lung. Latently mCMV-infected mice received pre-treatment with anti-NK1.1 monoclonal antibody, ganciclovir, or vehicle preceding lung IRI (Fig. 8A). One day after injury, both anti-NK1.1 and ganciclovir reduced total pulmonary NK cells relative to vehicle ($p = 0.007$ and $p = 0.01$, Fig. 8B) and similarly reduced adaptive NK cells ($p = 0.01$ for both, Fig. 8C). By 60 days, NK cell numbers in the ganciclovir group had returned to vehicle levels ($p = 0.94$), whereas the anti-NK1.1 group was reduced relative to vehicle ($p = 0.007$; Fig. 8B), with a similar pattern of adaptive NK cell counts in the ganciclovir ($p = 0.18$) and NK cell depletion groups ($p = 0.2$, Fig. 8C) relative to vehicle.

Despite this partial numerical recovery, the NK cells that repopulated the lung after depletion were phenotypically distinct. At 60 days, the Ly6C/KLRG1 subset composition of NK cells in anti-NK1.1-treated

mice differed markedly from vehicle ($p < 0.0001$), while ganciclovir-treated mice were indistinguishable from vehicle ($p = 0.41$; Fig. 8D). Unsupervised clustering of NK cell marker expression separated anti-NK1.1-treated samples from vehicle and ganciclovir (Fig. 8E). The same pattern held for tissue residency where vehicle and ganciclovir NK cells were predominantly CD49a+CD69 + and the residency composition was reset after NK cell depletion ($p < 0.0001$ versus vehicle (Fig. 8F). For the NKG2ACE/NKG2D compartment anti-NK1.1-treated lungs had more NKG2D relative to vehicle ($p < 0.0001$), and ganciclovir did not differ from vehicle ($p = 0.78$, Fig. 8G). Suppressing viral reactivation with ganciclovir therefore left the established pulmonary NK cell niche intact. In the NK cell-depleted group, the compartment repopulated with cells that lacked the resident, adaptive phenotype characteristic of the CMV-experienced lung.

Discussion

Here, in a cohort of nearly 700 lung transplant recipients and a mouse model of latent CMV, we found that latent CMV amplifies ALI through adaptive NK cells. Recipients with both latent donor CMV and severe PGD had the highest risk of CMV reactivation, the most severe impairment of gas exchange and ventilator mechanics, and a 3.7-fold increased hazard of death, none of which was explained by PGD or donor CMV alone. The mouse model reproduced these observations and traced the synergy to a durable population of tissue-resident, adaptive-like NK cells that were sufficient to propagate lung damage. Notably, adaptive NK cells were directly implicated in mortality, rather than with viral replication. Together, these data suggest that much of the early injury associated with CMV is mediated through an adaptive NK cell response rather than viral replication, identifying the NK cell compartment as a potential therapeutic target.

NK cells play diverse roles in allograft health that depend on tissue and temporal contexts [7]. For example, NKG2D activating receptor ligation may contribute to ALI through graft cytotoxicity [43–45] or may augment tolerance by culling of donor antigen-presenting cells thereby limiting indirect T cell receptor allorecognition [46]. NK cells bearing the activating receptor Ly49H in mice or NKG2C in humans are widely reported to constrain CMV morbidity in human patients [47,48] and mouse models [49]. In the mouse salivary gland, adaptive-like NK cells limit both the CD4 T cell population and propensity for autoimmunity [50]. In contrast, we previously demonstrated that human NKG2C + NK cells accumulated in lung before CMV DNAemia and were associated with over 4-fold increased risk for CLAD [17]. Here, we extend these findings, showing that adaptive-like NK cells in humans and mice carry cytotoxic transcriptional programs and that injury drives their accumulation and long-term persistence within the lung. Together, these findings suggest that organ injury may shift adaptive NK cell homeostasis toward a feed-forward loop of acute and chronic damage.

A central finding of this work is that ALI in the setting of latent CMV drives intense recruitment and retention of NK cells in the lung, linking injury to the acquisition of a tissue resident phenotype. NK cell tissue residency following CMV exposure has precedent in other organs. After primary mCMV infection,

circulating NK cells are recruited to the salivary glands in a CX3CR1-dependent manner and become established as a long-lived, tissue-resident memory-like population [50]. Adaptive-like NK cells with a tissue resident phenotype have also been described in human lung and blood [51]. Our findings differ in two respects: The resident program in the salivary gland is regulatory and protects the tissue from immune-mediated damage, whereas the resident adaptive NK cell population in the injured lung perpetuates injury. Second, the trigger in our setting is acute injury acting on latent virus, not primary infection. We previously showed that NK cells traffic to the small airways and alveolar compartment through CCR5 during IRI, and that CCR5 blockade reduces both NK cell migration and injury severity [52,53]. Here we extend that trafficking mechanism from recruitment to residency. Human lung adaptive-like NK cells produce the CCR5 ligand CCL5, and in the mouse model, NK cells co-localize with CCL5-rich regions of injured tissue. Because these cells also express CCR5, the pattern is consistent with an autocrine loop in which CCL5 produced by NK cells recruits and retains additional NK cells, leading to the observed adaptive NK aggregates. CXCR6, which binds CXCL16 expressed at sites of epithelial injury, is a major tissue-retention signal for lung lymphocytes and likely reinforces this process [54]. Together, these signals may convert transient, injury-driven recruitment into a self-sustaining resident program that persists beyond the initial insult.

Our findings challenge the prevailing view that CMV-associated injury after transplantation is primarily a consequence of viral replication and dissemination [55,56]. Instead, they suggest that a significant driver of lung injury and mortality is the adaptive immune program established after viral reactivation. Although multiple lymphocyte populations contribute to CMV control, their responses to acute injury differed markedly [57]. CD8 and γδ T cell expansion correlated with the duration of latent infection, consistent with an antigen-driven memory response [58], whereas the injurious NK cell expansion occurred as a consequence of both acute injury and latent infection. The compartment that propagated injury was therefore uncoupled from the conventional antiviral response. This notion was exemplified by treatment with ganciclovir, which blunted viral replication, yet did not prevent injury or improve survival, even when CMV replication was reduced. This mirrors the clinical experience in lung transplantation, where antiviral prophylaxis reduces CMV disease, but the associated risk CLAD and death persists [3,59]. If suppressing replication does not remove the risk, replication alone is unlikely to be the proximate cause. Together, our data support the paradigm where 1) acute injury reactivates latent CMV, plausibly through TNFα released during ischemia-reperfusion, a known trigger of viral reactivation [60]; and 2) reactivation then establishes and sustains an adaptive NK cell program that perpetuates tissue injury. In this model, CMV initiates the response but is not the direct effector of tissue damage. These findings suggest that the adaptive NK program, rather than viral replication itself, may represent the more relevant therapeutic target.

This study has several strengths. The human cohort is among the largest assembled to examine CMV and PGD together, and the competing-risks framework separated death attributable to the CMV-PGD interaction from death driven by either exposure alone. Pairing the cohort with a latent CMV mouse model allowed us to move from association to mechanism, and adoptive transfer and depletion experiments provide direct evidence that the adaptive NK compartment contributes directly to injury. The

dissociation between mortality and viral load is clinically relevant, motivating the study of CMV prophylaxis regimens that prevent adaptive NK cell amplification, rather than suppress viral load *per se*. Our study also has limitations. The human analyses are observational, and unmeasured factors could contribute to the associations we report, though the complementary mouse experiments partially mitigate this concern. CMV reactivation and PGD were defined from clinical data and are subject to measurement error and our single-center clinical protocols, which may defer from other centers. We did not resolve the effector mechanism by which the adaptive NK compartment propagates injury. We previously showed that NKG2D mediates NK cell-dependent IRI, making the same axis a plausible candidate here; however, our data do not exclude contributions from other activating receptors or receptor-independent effector functions, and multiple pathways may operate in concert.

In summary, we identify a durable adaptive NK cell program that links latent CMV to mortality after lung transplantation. ALI reactivated latent CMV and expanded tissue-resident adaptive NK cells that persisted well beyond the initial insult. Across human and mouse studies, this adaptive NK program, rather than viral replication, was associated with lung injury and mortality. NK cell depletion prevented injury and improved survival, whereas ganciclovir did not, suggesting that the adaptive NK compartment is a more relevant therapeutic target than viral replication alone. Our recent development of a depleting anti-CD94 antibody provides one potential strategy to test this concept in human disease [61]. Although these studies were performed in the context of lung transplantation, the biology is relevant beyond this setting. Acute injury is a well-recognized trigger of CMV reactivation across multiple forms of critical illness and solid organ transplantation [62–64], and tissue-resident adaptive NK cells have been described in both human and experimental systems. Whether similar injury-induced adaptive NK cell programs contribute to CMV-associated pathology after other forms of organ injury or in other solid organ allografts remains to be determined. In addition, whether targeting adaptive NK cells can safely improve outcomes after transplantation remains an important question for future studies.

Materials and Methods

Human study population, clinical data and clinical definitions.

Consenting adult lung allograft recipients transplanted between April 2010, and June 2023 were included in the study (**Supplemental Fig. 1**), in accordance with the approved institutional review board protocol #13-10738. Recipient clinical data including mechanical ventilator parameters, CMV plasma polymerase chain reaction (PCR) values, other laboratory results, and baseline characteristics were extracted from electronic medical records. Standard clinical protocols including induction medication regimens and early post-operative clinical care were detailed previously [45,65].

CMV DNAemia was identified by quantitative plasma PCR performed per institutional surveillance protocol [17]. The primary time-to-event outcome was first detection of CMV DNAemia within the first post-transplant year. CMV reactivation severity was graded ordinally based on peak viral load: no

DNAemia, detected below quantification limit, < 1,000 IU/mL, 1,000–5,000 IU/mL, > 5,000 IU/mL, and very high grade.

Severe PGD was defined by international criteria as the presence of bilateral pulmonary opacities on chest radiography and PaO_2/FiO_2 <200 mmHg or extracorporeal membrane oxygenation use on post-operative day 2 or post-operative day 3 [23,66]. Donor and recipient CMV serostatus was determined by clinical CMV-specific immunoglobulin G (IgG) serologies. Driving pressure was defined as the difference between plateau pressure and positive end expiratory pressure (PEEP). Chronic lung allograft dysfunction (CLAD) was defined in accordance with international criteria, as shown previously [66,67].

Mice and animal protocol.

All animal experiments were performed in accordance with institutional guidelines and were approved by the Institutional Animal Care and Use Committee (IACUC) at the University of California, San Francisco under protocol #AN210987. Male and female C57BL/6J mice (8–10 weeks old) were obtained from Jackson Laboratories (#000664, Bar Harbor, ME) and housed under pathogen-free conditions or under Animal Biosafety Level 2 (ABSL-2) conditions.

Mouse cytomegalovirus infection latency model with ischemia reperfusion injury.

Mice were infected intraperitoneally with mouse cytomegalovirus (mCMV, Smith strain) [68] at a dose of 1×10^5 plaque-forming units (PFU) diluted in sterile phosphate-buffered saline (PBS). Mock-infected control mice received an equivalent volume of sterile PBS. Mice were allowed to recover and progress to viral latency for 60 days following primary infection. CMV latency was confirmed by the absence of immediate early 1 (IE-1) gene transcript copies by PCR. At 65 days post-mCMV or mock infection, mice underwent either warm lung ischemia reperfusion injury (IRI) or sham surgery, performed by a trained microvascular surgeon as previously described [44,53]. Briefly, following a left thoracotomy a slipknot silk suture was tied (hilar clamp) or left untied (sham) around the left hilum for 2 hours. The suture was removed and animals were euthanized at 4 hours, 1 day, or 60 days. In select experiments, acute lung injury was induced via intratracheal instillation of 1 mg/kg lipopolysaccharide (LPS) resuspended in 50 µL of PBS, as previously described [33].

Quantification of mouse CMV gene expression.

Mouse cytomegalovirus (mCMV) DNA was quantified by real-time PCR (qPCR) targeting the viral immediate-early 1 (*IE1*) gene. Genomic DNA from mCMV infected mice was extracted from peripheral blood using the ReliaPrep Blood gDNA Miniprep System (#A5082, ProMega, Madison, WI) and from tissues using DNeasy Blood & Tissue Kit (Qiagen #69504) according to the manufacturers' instructions. Quantitative PCR was performed (#11762-500, Invitrogen) with mCMV IE1-specific primers (Forward: 5'-AGCCACCAACATTGACCACGCAC-3'; Reverse: 5'-GCCCCAACCAGGACACACAACTC-3'). Absolute viral DNA copy numbers were determined using a standard curve generated from serial dilutions (2×10^5 to 2

copies/μL) of an mCMV IE1-containing plasmid standard. Viral DNA copy numbers were calculated by comparison with the plasmid standard curve and expressed as mCMV genome copies per sample.

Pharmacologic and antibody treatments.

To evaluate the contribution of latent mouse cytomegalovirus (mCMV) infection to ischemia–reperfusion (IR)-induced ALI and to assess the efficacy of antiviral and immune-modulating therapies, latently mCMV-infected mice were randomly assigned to receive i.p. anti-mouse anti-NK1.1 monoclonal antibody (10 mg/kg, #BE0036, BioXCell, Lebanon, NH), ganciclovir (10 mg/kg, #S1878, Selleckchem, Houston, TX), or vehicle control. Treatments were administered by intraperitoneal injection 24 hours prior to lung ischemia–reperfusion injury. For long-term therapeutic studies, latent mCMV-infected mice received Cytogam, anti-NK1.1, GCV, or vehicle control by intraperitoneal injection weekly for two consecutive weeks.

Tissue processing and lung injury assessments.

Data were collected through 60 days post reperfusion (125 days post infection). Tissues including lung, spleen, heart, liver, salivary gland, and blood were collected. Lung tissues were digested to single cell suspensions in 1 mL PBS containing collagenase D (2 mg/mL, #11088858001, Sigma-Aldrich, St. Louis, MO) and 10 μL of DNase I (10 μg/μL, #10104159001, Sigma-Aldrich), as previously described [33]. Single left lung bronchoalveolar lavage (BAL) was performed with 100 μL of gentle PBS lavage. BAL protein was quantified with the BCA protein assay (#A55864, Thermo Fisher Scientific, Waltham, MA). Arterial blood PaO_2 was assessed in mmHg using an i-STAT 1 Handheld Analyzer and VetScan CG4 i-STAT Cartridges (#89126, Abaxis, Union City, CA). For histological analysis, lungs were formalin-fixed and paraffin-embedded (FFPE) prior to sectioning and hematoxylin and eosin (H&E) staining. Digital slide images were scanned and visualized with QuPath software [69]. Lung histologic injury was scored using an IRI system by an expert pathologist (FL), assessing edema, red blood cell extravasation, and neutrophils in the alveolar and interstitial spaces and endothelial barrier failure.

Mouse spectral flow cytometry for NK, and T cell phenotyping

Cells were washed and resuspended in flow cytometry buffer (# E554656, Becton Dickinson, Franklin Lakes, NJ). Single-cell suspensions of lung tissue were stained with a comprehensive spectral flow cytometry panel (**Supplemental Table 2**) to identify and phenotype lymphocyte populations, including NK cells, T cells, and other immune subsets, as previously described. Data were acquired on an Aurora spectral flow cytometer (Cytek, Fremont, CA) and analyzed using FCS Express software (version 7, De Novo Software, Pasadena, CA). Cell populations were gated according to **Supplemental Fig. 3**. NK cell phenotypes were assessed for activation, cytotoxicity, tissue residency and adaptive-associated markers.

Ly49H + NK cell adoptive transfer experiments

Spleens from latently CMV-infected C57BL/6 donor mice (65 days post-CMV infection) were collected and mechanically dissociated, passed through a 70-μm mesh filter, pelleted, and resuspended at 1 × 10^8 nucleated cells/mL. NK cells were stained and sorted by fluorescence-activated cell sorting into $Ly49H^+$ and $Ly49H^-$ fractions, with purity confirmed by flow cytometry. Sorted $Ly49H^+$ or $Ly49H^-$ NK cells were injected intraperitoneally (1 × 10^6) into *Il2rg*$^{-/-}$*Rag2*$^{-/-}$ recipients. Five days later, mice underwent ALI preceding endpoint assessments.

Spatial transcriptomics, data processing, annotation, and analysis

FFPE mouse lung blocks were submitted to Signios Bio (Redwood City, CA) for 10x Genomics Visium HD spatial gene expression profiling. Latently mCMV-infected lungs were profiled at 6 hours (sham n = 1, IRI n = 2) and 60 days (sham n = 2, IRI n = 2) after surgery, for seven sections total. Sectioning, H&E imaging, probe hybridization, capture, library preparation, and sequencing were performed by the vendor using the standard Visium HD FFPE workflow. Reads were aligned and counted with Space Ranger against the mouse reference transcriptome, and the 2 μm capture data were aggregated into bins for analysis.

Binned expression matrices were quality-filtered to remove low-count bins, normalized, and dimensionally reduced, and bins were clustered and annotated to 12 lung cell-type populations (AT1, AT2, airway/club, endothelial, fibroblast, smooth muscle, macrophage, neutrophil, lymphatic, T cell, NK cell, and B cell) using canonical lineage marker genes, with the top markers supporting each annotation shown in **Supplemental Fig. 9**. Cell-type composition per section was expressed as the fraction of total bins.

Spatial organization of the NK cell compartment was assessed against a permutation-based null in which bin labels were randomly reassigned within each section. NK cell aggregation was quantified as the ratio of observed-to-expected NK-to-NK cell bin density and by comparison of observed NK cell nearest-neighbor distances to the permuted distribution. For each cell type, the median Euclidean distance (μm) from NK bins to the nearest bin of that type was computed per condition. To characterize the NK cell signaling neighborhood, proximity enrichment (observed/expected) was calculated for secreted and contact-dependent ligand transcripts in the local NK cell neighborhood and tested against the permuted spatial null, comparing IRI and sham at 60 days. Enrichment was similarly computed for collagen-transcript regions and for curated and MSigDB Hallmark gene-set programs.

Statistical Analysis

Cumulative incidence of lung transplant recipient CMV DNAemia was plotted by exposure group. The association between donor CMV seropositivity stratified by severe PGD and time to first CMV DNAemia was evaluated using Cox proportional hazards regression. The association between exposure group and CMV reactivation severity grade was evaluated using ordinal logistic regression. Time to CLAD and death were modeled jointly as competing risks using cause-specific Cox proportional hazards regression, with CLAD and death as competing events, donor CMV serostatus and severe PGD as the combined

exposure. All models were adjusted for age, sex, ethnicity, transplant type, and transplant group. Missing covariate data were addressed using multiple imputation, with less than 5% of data imputed.

Mouse data are shown as median with interquartile range with individual animals as points. All tests were two-sided with significance at $p < 0.05$. For two-group comparisons of continuous endpoints, such as viral copy numbers, and total NK cell and adaptive NK cell counts, differences were assessed by the Mann-Whitney U test. Where comparisons spanned multiple groups, endpoints were compared by Kruskal-Wallis with Dunn's post hoc testing while NK and T cell immunophenotyping comparisons of sham versus IRI within each CMV and timepoint stratum used Mann-Whitney U testing with Benjamini-Hochberg adjustment. Cell subset composition distributions were compared by chi-square test with Monte Carlo simulation, including comparisons of treatment groups to vehicle. Differences in mouse experimental group 30-day survival were calculated by log-rank test with pairwise comparisons, and spatial NK organization and neighborhood enrichment were evaluated against a permutation-based spatial null.

All analyses and data plots were performed using R statistical programming software (version 4.4, R) with libraries "survival," "survminer," "MASS," "mice," "mgcv," "ggpubr," "foreign," "stringr," "multcomp," "dplyr," "tidyr," "ggplot2," "patchwork," "pheatmap," "RColorBrewer," "Seurat," "CellChat," "msigdbr," "openxlsx," and "dunn.test."

Declarations

Contributions

Conceptualization: MRL, DRC; Methodology: RB, OAA, NM, LQ, JRG, DRC; Software: DRC; Validation: RB, DRC; Formal Analysis: RB, JRG, DRC; Investigation: RB, OAA, NM, DZ, FL, A.Sc, A.Sh, LQ; Resources: JPS, SRH, MRL, JRG, DRC; Data Curation: RB, DZ, JPS, DRC; Writing - Original Draft: RB, JRG, DRC; Writing - Review & Editing: all authors; Visualization: NM, DRC; Supervision: MRL, JRG, DRC; Project Administration: JRG, DRC; Funding Acquisition: MRL, JRG, DRC.

Funding Support

D.R.C. receives investigator-initiated grant support from Kamada and investigator-initiated research support from Natera, serves on an advisory board for Incyte, and previously received investigator-initiated grant support from DrenBio. None of these entities had any role in this study. The remaining authors declare no competing interests. This work was supported by the VA Office of Research and Development awards 1IK2BX005301 (DRC) and CX002011 (JRG); the American Lung Association, the Cystic Fibrosis Foundation CALABR19Q0 (DRC), and the NIH R01HL179747 (DRC). MRL and LQ were supported by NIH (R35HL161241). DZ and LQ were also supported by the Nina Ireland Program for Lung Health (UCSF). We acknowledge the Parnassus Flow Cytometry Core (RRID:*SCR 018206*) supported in part by Grant NIH P30 DK063720 and by the NIH S10 Instrumentation Grant S10 1S10OD026940-01.

Acknowledgements

We thank Lewis L. Lanier for advice and manuscript review. We thank members of the Aguilar lab for their assistance with reagents, experimental design, and for their scientific discourse and support. We thank the UCSF flow cytometry core for their instrumental assistance in designing and implementing the spectral flow cytometry panels. We are thankful to the other members of the Calabrese and Greenland laboratory groups for their expert discussion and suggestions.

Data availability

Sequencing data generated in this study will be deposited in the Gene Expression Omnibus under accession () with public release upon publication. Individual-level clinical data contain protected health information and cannot be shared publicly. De-identified data are available to qualified investigators under a data use agreement, and requests should be directed to the corresponding author

Code availability

Analyses were performed in R using publicly available packages as described in the Methods, with versions and parameters specified therein. Custom R scripts supporting the findings are available from the corresponding author on request.

References

1. Staras SA et al (2006) Seroprevalence of cytomegalovirus infection in the United States, 1988–1994. Clin Infect Dis 43:1143–1151
2. Balthesen M, Dreher L, Lučin P, Reddehase MJ (1994) The establishment of cytomegalovirus latency in organs is not linked to local virus production during primary infection. J Gen Virol 75:2329–2336
3. Paraskeva M et al (2011) Cytomegalovirus replication within the lung allograft is associated with bronchiolitis obliterans syndrome. Am J Transpl 11:2190–2196
4. Brehm MA et al (2010) Allografts Stimulate Cross-Reactive Virus-Specific Memory CD8 T Cells with Private Specificity. Am J transplantation: official J Am Soc Transplantation Am Soc Transpl Surg 10:1738–1748
5. Che JW, Daniels KA, Selin LK, Welsh RM (2017) Heterologous Immunity and Persistent Murine Cytomegalovirus Infection. J Virol 91
6. Qiu Z et al (2015) Cytomegalovirus-Based Vaccine Expressing a Modified Tumor Antigen Induces Potent Tumor-Specific CD8(+) T-cell Response and Protects Mice from Melanoma. Cancer Immunol Res 3:536–546
7. Calabrese DR, Lanier LL, Greenland JR (2019) Natural killer cells in lung transplantation. Thorax 74:397–404

8. Gumperz JE, Parham P (1995) The enigma of the natural killer cell. Nature 378:245–248
9. Lanier LL (2005) NK cell recognition. Annu Rev Immunol 23:225–274
10. Cook KD, Whitmire JK (2013) The depletion of NK cells prevents T cell exhaustion to efficiently control disseminating virus infection. J Immunol 190:641–649
11. Mujal AM, Delconte RB, Sun JC (2021) Natural Killer Cells: From Innate to Adaptive Features. Annu Rev Immunol 39:417–447
12. Braud VM et al (1998) HLA-E binds to natural killer cell receptors CD94/NKG2A, B and C. Nature 391:795–799
13. Adams NM et al (2019) Cytomegalovirus Infection Drives Avidity Selection of Natural Killer Cells. Immunity 50:1381–1390e1385
14. McQueen KL, Freeman JD, Takei F, Mager DL (1998) Localization of five new Ly49 genes, including three closely related to Ly49c. Immunogenetics 48:174–183
15. Daniels KA et al (2001) Murine cytomegalovirus is regulated by a discrete subset of natural killer cells reactive with monoclonal antibody to Ly49H. J Exp Med 194:29–44
16. Smith HR et al (2002), *Recognition of a virus-encoded ligand by a natural killer cell activation receptor. Proc. Natl. Acad. Sci. U. S. A. 99, 8826–8831*
17. Calabrese DR et al (2019) NKG2C Natural Killer Cells in Bronchoalveolar Lavage Are Associated With Cytomegalovirus Viremia and Poor Outcomes in Lung Allograft Recipients. Transplantation 103:493–501
18. Ishiyama K et al (2022) Mass cytometry reveals single-cell kinetics of cytotoxic lymphocyte evolution in CMV-infected renal transplant patients. *Proc. Natl. Acad. Sci. U. S. A.* 119
19. Gotts JE et al (2019) Clinically relevant model of pneumococcal pneumonia, ARDS, and nonpulmonary organ dysfunction in mice. Am J Physiol Lung Cell Mol Physiol 317:L717–l736
20. Kulkarni HS et al (2022) Update on the Features and Measurements of Experimental Acute Lung Injury in Animals: An Official American Thoracic Society Workshop Report. Am J Respir Cell Mol Biol 66:e1–e14
21. Matute-Bello G et al (2011) An official American Thoracic Society workshop report: features and measurements of experimental acute lung injury in animals. Am J Respir Cell Mol Biol 44:725–738
22. Matute-Bello G, Frevert CW, Martin TR (2008) Animal models of acute lung injury. Am J Physiol Lung Cell Mol Physiol 295:L379–L399
23. Snell GI et al (2017) Report of the ISHLT Working Group on Primary Lung Graft Dysfunction, part I: Definition and grading; A 2016 Consensus Group statement of the International Society for Heart and Lung Transplantation. J Heart Lung Transpl 36:1097–1103
24. Morrison MI, Pither TL, Fisher AJ (2017) Pathophysiology and classification of primary graft dysfunction after lung transplantation. J Thorac Dis 9:4084–4097
25. Ranieri VM et al (2012) Acute respiratory distress syndrome: the Berlin Definition. JAMA 307:2526–2533

26. Ashbaugh DG, Bigelow DB, Petty TL, Levine BE (1967) Acute respiratory distress in adults. Lancet 2:319–323
27. Bellani G et al (2016) Patterns of Care, and Mortality for Patients With Acute Respiratory Distress Syndrome in Intensive Care Units in 50 Countries. JAMA 315:788–800Epidemiology
28. Johnson ER, Matthay MA (2010) Acute lung injury: epidemiology, pathogenesis, and treatment. J Aerosol Med Pulm Drug Deliv 23:243–252
29. Van Slambrouck J et al (2022) A Focused Review on Primary Graft Dysfunction after Clinical Lung Transplantation: A Multilevel Syndrome. *Cells* 11
30. Daoud D et al (2021) Incidence of primary graft dysfunction is higher according to the new ISHLT 2016 guidelines and correlates with clinical and molecular risk factors. J Thorac Dis 13:3426–3442
31. Calabrese DR et al (2021) Natural killer cells activated through NKG2D mediate lung ischemia-reperfusion injury. J Clin Invest 131
32. Calabrese DR et al (2022) NKG2D receptor activation drives primary graft dysfunction severity and poor lung transplantation outcomes. JCI Insight
33. Bharti R, Greenland N, Cleary SJ, Greenland JR, Calabrese DR (2026) CCR5 + NK cells drive hypoxemia in endotoxin-induced acute lung injury. Am J Respir Cell Mol Biol
34. Steinmüller C et al (1997) Analysis of leukocyte activation during acute rejection of pulmonary allografts in noninfected and cytomegalovirus-infected rats. J Leukoc Biol 61:40–49
35. Mutimer DJ, Shaw J, O'Donnell K, Elias E (1997) Enhanced (cytomegalovirus) viral replication after transplantation for fulminant hepatic failure. Liver Transpl Surg 3:506–512
36. Lee KH et al (2022) Association of cytomegalovirus diseases with newly developed myocardial infarction and congestive heart failure: data from a national population-based cohort. Arch Med Sci 18:1188–1198
37. Lanier LL, Corliss B, Wu J, Phillips JH (1998) Association of DAP12 with activating CD94/NKG2C NK cell receptors. Immunity 8:693–701
38. Carretero M, Llano M, Navarro F, Bellón T, López-Botet M (2000) Mitogen-activated protein kinase activity is involved in effector functions triggered by the CD94/NKG2-C NK receptor specific for HLA-E. Eur J Immunol 30:2842–2848
39. Kawashima M et al (2024) Association between cytomegalovirus viremia and long-term outcomes in lung transplant recipients. Am J Transpl 24:1057–1069
40. Calabrese DR et al (2024) Macrophage and CD8 T cell discordance are associated with acute lung allograft dysfunction progression. J Heart Lung Transpl
41. Schlums H et al (2015) Cytomegalovirus infection drives adaptive epigenetic diversification of NK cells with altered signaling and effector function. Immunity 42:443–456
42. Brunet-Ratnasingham E et al (2025) Persistent and progressive acute lung allograft dysfunction is linked to cell compositional and transcriptional changes in small airways. J Heart Lung Transpl 44:1482–1492

43. Aguilar OA et al (2023) MICB Genomic Variant is Associated with NKG2D-mediated Acute Lung Injury and Death. Am J Respir Crit Care Med
44. Calabrese DR et al (2021) Natural killer cells activated through NKG2D mediate lung ischemia-reperfusion injury. J Clin Invest 131:e137047
45. Calabrese DR et al (2022) NKG2D receptor activation drives primary graft dysfunction severity and poor lung transplantation outcomes. JCI Insight 7:e164603
46. Jungraithmayr W et al (2013) Cytokine complex-expanded natural killer cells improve allogeneic lung transplant function via depletion of donor dendritic cells. Am J Respir Crit Care Med 187:1349–1359
47. Ataya M et al (2020) Pretransplant adaptive NKG2C + NK cells protect against cytomegalovirus infection in kidney transplant recipients. Am J Transpl 20:663–676
48. Lopez-Verges S et al (2011), *Expansion of a unique CD57(+)NKG2Chi natural killer cell subset during acute human cytomegalovirus infection. Proc. Natl. Acad. Sci. U. S. A. 108, 14725–14732*
49. Sun JC, Beilke JN, Lanier LL (2009) Adaptive immune features of natural killer cells. Nature 457:557–561
50. Schuster IS et al (2023) Infection induces tissue-resident memory NK cells that safeguard tissue health. Immunity 56:531–546e536
51. Brownlie D et al (2021) Expansions of adaptive-like NK cells with a tissue-resident phenotype in human lung and blood. *Proc. Natl. Acad. Sci. U. S. A.* 118
52. Bharti R et al (2024), *CCR5 Drives NK Cell Mediated Airway Damage in an Endotoxin-induced Model of Acute Lung Injury. AJRCCM 209, A6837-A6837*
53. Santos J et al (2023) CCR5 drives NK cell-associated airway damage in pulmonary ischemia-reperfusion injury. JCI Insight
54. Wein AN et al (2019) CXCR6 regulates localization of tissue-resident memory CD8 T cells to the airways. J Exp Med 216:2748–2762
55. Balfour HH (1979) Jr. Cytomegalovirus: The Troll of Transplantation. Arch Intern Med 139:279–280
56. Kotton CN et al (2025) The Fourth International Consensus Guidelines on the Management of Cytomegalovirus in Solid Organ Transplantation. Transplantation 109:1066–1110
57. Bharti R, Calabrese DR (2024) Innate and adaptive effector immune drivers of Cytomegalovirus disease in lung transplantation: a double-edged sword. Front Transplantation 3
58. Pickering H et al (2025) Cytomegalovirus-associated CD57 + KLRG1 + CD8 + TEMRA T cells are associated with reduced risk of CMV viremia in kidney transplantation and chronic allograft dysfunction in lung transplantation. Hum Immunol 86:111285
59. Wiita AP et al (2012) Cytomegalovirus disease and infection in lung transplant recipients in the setting of planned indefinite valganciclovir prophylaxis. Transpl Infect Dis 14:248–258
60. Prösch S et al (1995) Stimulation of the human cytomegalovirus IE enhancer/promoter in HL-60 cells by TNFalpha is mediated via induction of NF-kappaB. Virology 208:197–206

61. Tsao T et al (2024) CD94 + Natural Killer cells potentiate pulmonary ischemia-reperfusion injury. Eur Respir J 64:2302171
62. Ong DSY et al (2016) Cytomegalovirus reactivation and mortality in patients with acute respiratory distress syndrome. Intensive Care Med 42:333–341
63. Silva TF et al (2019) Reactivation of Cytomegalovirus Increases Nitric Oxide and IL-10 Levels in Sepsis and is Associated with Changes in Renal Parameters and Worse Clinical Outcome. Sci Rep 9:9016
64. Zhang Z et al (2019) A clinically relevant murine model unmasks a two-hit mechanism for reactivation and dissemination of cytomegalovirus after kidney transplant. Am J Transpl 19:2421–2433
65. Calabrese DR et al (2018) Genotypes associated with tacrolimus pharmacokinetics impact clinical outcomes in lung transplant recipients. Clin Transpl 32:e13332
66. Greenland JR et al (2026) Considerations for Endpoints in Lung Transplant Clinical Trials: An ISHLT Consensus Statement. J Heart Lung Transpl 45:e104–e128
67. Calabrese DR et al (2023) CD16(+) natural killer cells in bronchoalveolar lavage are associated with antibody-mediated rejection and chronic lung allograft dysfunction. Am J Transpl 23:37–44
68. Potempa M et al (2022) Influence of Self-MHC Class I Recognition on the Dynamics of NK Cell Responses to Cytomegalovirus Infection. J Immunol 208:1742–1754
69. Bankhead P et al (2017) Open source software for digital pathology image analysis. Sci Rep 7:16878QuPath

Figures

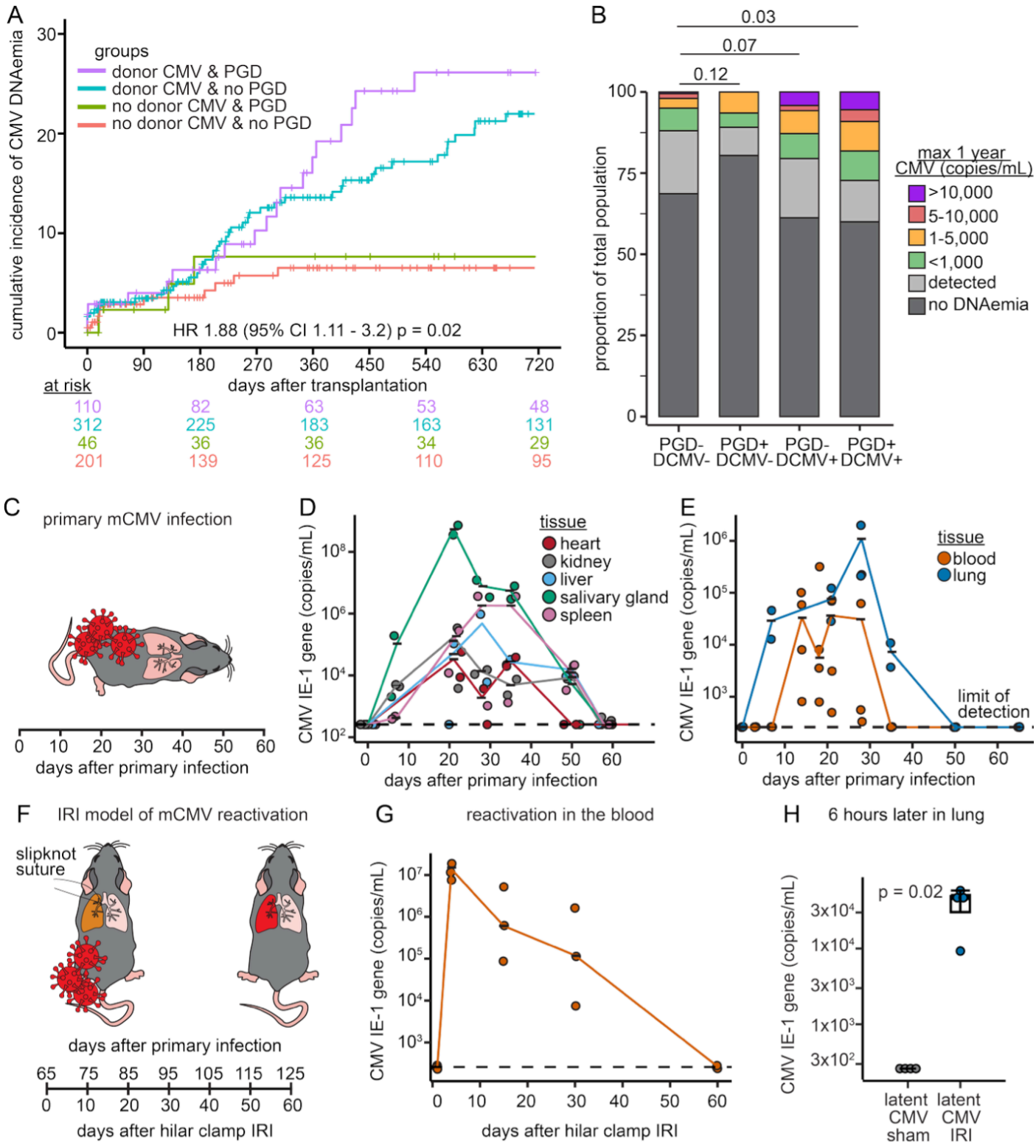


Figure 1

Latent donor cytomegalovirus and severe PGD drive viral reactivation. (A) Cumulative incidence plot of CMV DNAemia over the first post-transplant year in 669 lung transplant recipients stratified by donor CMV serostatus and severe PGD. Tick marks indicate censored observations. **(B)** Proportional distribution of first-year CMV DNAemia severity grades across the four exposure groups. Severity categories reflect maximum viral load: no DNAemia (dark gray), detected at lower limit of assay (light

gray), above detected but <1,000 copies/mL (green), 1,000–5,000 copies/mL (orange), 5,000-10,000 copies/mL (pink), >10,000 copies (purple). (**C)** Schematic of primary mCMV infection model. **(D)** Longitudinal CMV viral kinetics in individual mice following primary mCMV inoculation in solid organs (n = 2 per timepoint) and in **(E)** blood and lung (n = 3-4 per timepoint). **(F)** Schematic of the left lung hilar clamp model of mCMV reactivation after ischemia-reperfusion injury (IRI) in latently infected mice. **(G)**Blood CMV IE-1 gene copies following lung IRI. **(H)** Lung tissue mCMV IE-1 gene copies obtained 6 hours following sham or IRI surgeries. Differences in cumulative incidence of CMV DNAemia or maximum viral load were calculated with Cox proportional hazards or ordinal logistic regression, respectively, adjusted for age, sex, ethnicity, transplant type, and transplant group. Mouse model differences calculated with Mann-Whitney U testing.

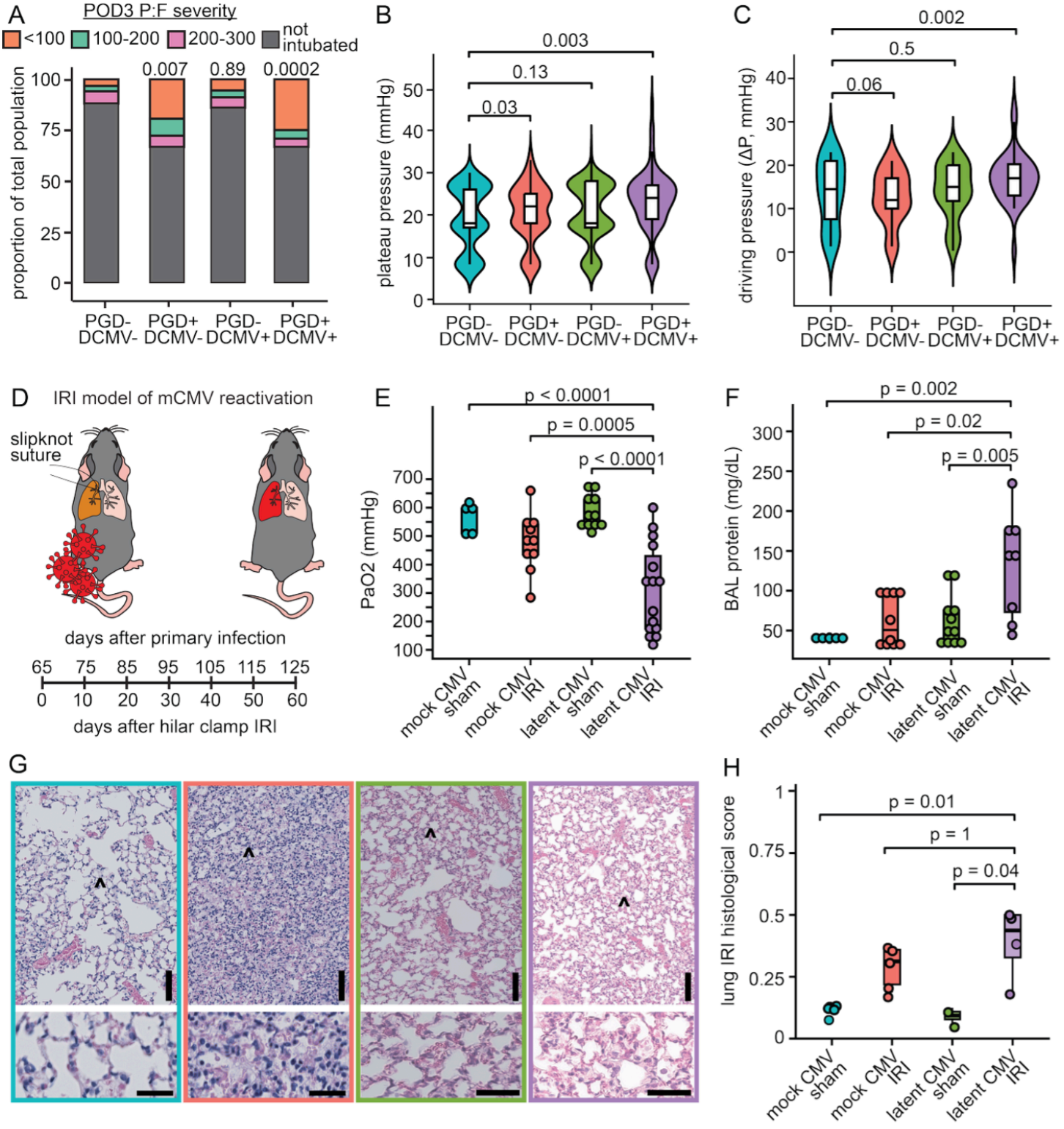


Figure 2

Latent CMV is associated with worse acute lung injury in humans and experimental models. Acute lung injury severity on post operative day 3 (POD3) stratified by donor CMV status and severe PGD are shown by **(A)** proportional bar plot distribution of PaO_2:FiO_2 (P:F) ratio, **(B)** ventilator plateau pressure in mm Hg, and **(C)** driving pressure (plateau pressure – positive end expiratory pressure [ΔP], mm Hg) in the clinical cohort.

(D) Schematic of the experimental mouse model of lung injury with and without CMV exposure and with (ischemia reperfusion injury [IRI]) and without (sham) acute lung injury. Lung injury was quantified across CMV and IRI groups by **(E)** arterial PaO2, **(F)** bronchoalveolar lavage (BAL) protein, and **(G)** representative histologic injury shown in two magnifications with bars representing 100 um and ^ showing higher magnification area. At least n = 5 mice were used per condition. Data are presented as violin plots (**B** & **C**) or boxplots with median and interquartile range, individual data points are shown for mouse work. Human data were analyzed ordinal regression adjusted for baseline characteristics, and mouse data were analyzed with Kruskal-Wallis with Dunn's post hoc testing to account for multiple comparisons.

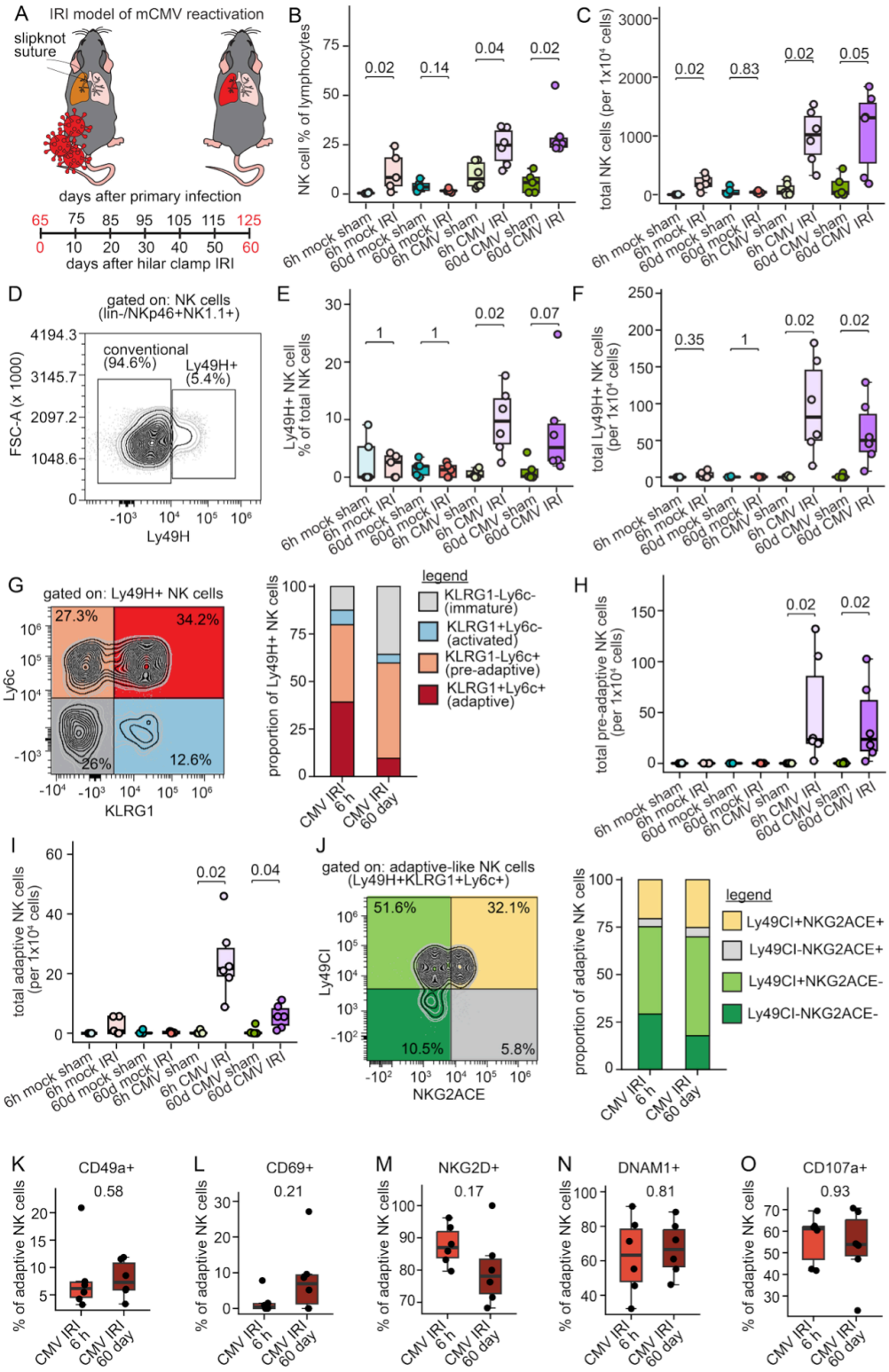


Figure 3

Pulmonary adaptive-like NK cells are increased and persist after IRI-induced CMV reactivation. (A) Schematic of the mouse IRI model of mCMV reactivation. Latently infected or mock-infected C57BL/6 mice underwent lung IRI or sham surgery and endpoints were collected 6 hours or 60 days after procedures. Across mCMV and IRI groups, lung NK cells were quantified as **(B)** a percentage of total lymphocytes or **(C)** a total cell count**. (D)** Representative contour plot of the CMV receptor, Ly49H, in

isolated NK cells. Ly49H+ NK cells were quantified across groups **(E)** a percentage of total lymphocytes or **(F)** a total cell count. **(G)** Gating strategy for identifying pre-adaptive (Ly49H+KLRG1-Ly6c+) or adaptive (Ly49H+KLRG1+Ly6c+) NK cells with median normalized stacked bar plot depicting relative frequencies. Given the paucity of Ly49H+ NK cells in other groups, adaptive NK cells were quantified in mCMV IRI groups by **(H)**percentage of total NK cells or **(I)** a total cell count**. (J)**Countour plot showing Ly49CI and NKG2ACE across the adaptive NK cell subset with median normalized stacked bar plot depicting relative frequencies of licensed and educated cells. Frequencies of adaptive NK cells expressing **(K)** CD49a, **(L)** CD69, **(M)**NKG2D, **(N)** DNAM1 and **(O)** CD107a are shown across mCMV IRI timepoints. Data are shown as median with IQR with n=5–6 mice per condition. Comparisons between IRI and sham across mCMV groupings were performed using the Wilcoxon rank-sum test adjusted for false discovery with the Benjamini-Hochberg approach. Stacked bar plots show median normalized subgroup composition between CMV IRI 6h and CMV IRI 60d groups.

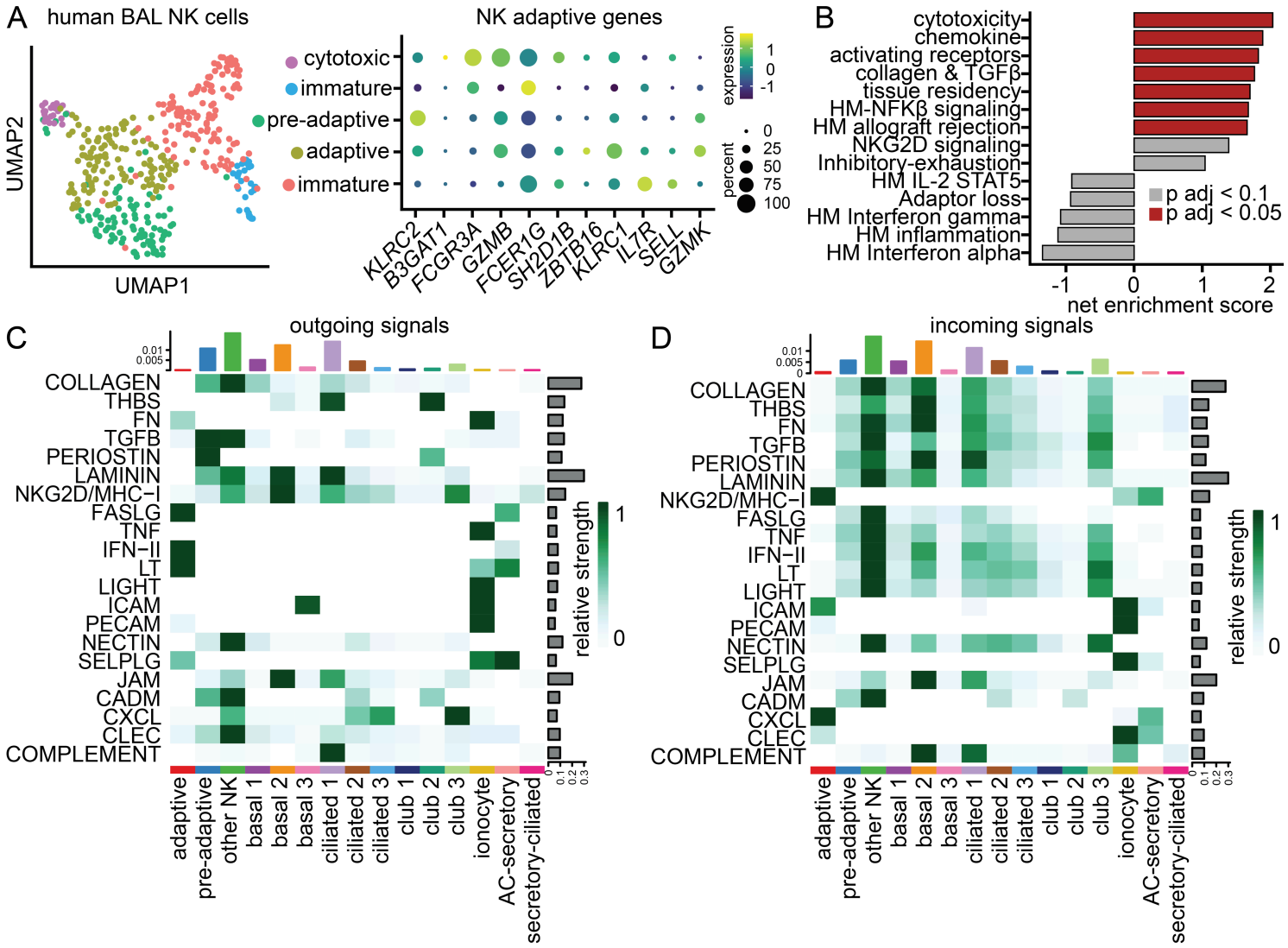


Figure 4

Human bronchoalveolar lavage NK cells contain an adaptive subset with tissue-residency and allograft-rejection signaling programs. Bronchoalveolar lavage from 45 lung transplant recipients were analyzed

by single cell RNA sequencing. **(A)** UMAP of NK cells from recipient BAL colored by NK cell subset (left). Dot plot of canonical NK maturation and adaptive-identity genes (right) across subsets. **(B)** Net gene enrichment scores for selected gene sets comparing adaptive subsets to other NK cell subsets. Cell-cell communication pathways were compared between NK cell subsets and epithelial subsets quantified in bronchiolar brushes (n = 17). (**C)** Outgoing and**(D)** incomingsignaling across NK subsets (adaptive, pre-adaptive, other NK) and airway epithelial populations are shown.

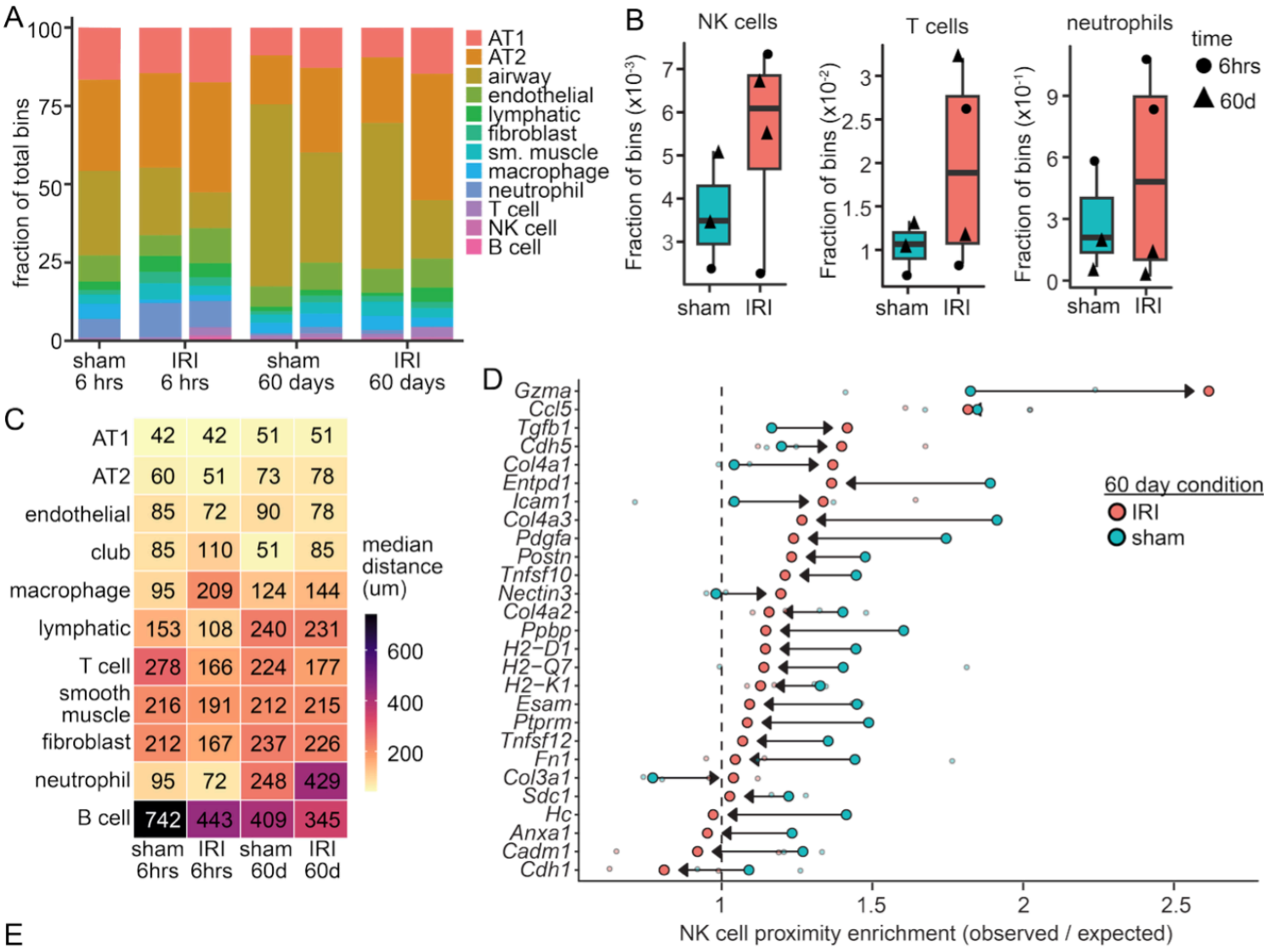


Figure 5

Spatial organization and signaling neighborhood of NK cells in mouse. We spatially profiled latent CMV lungs at 6 hours after sham and IRI (n = 1, n = 2, respectively) and 60 days after sham and IRI (n = 2 each). (**A**) Cell-type composition of each section (fraction of total bins) for sham and IRI lungs at 6 hours and 60 days, across 12 annotated populations. (**B**) Bin fractions of NK cells, T cells, and neutrophils in sham versus IRI; point shape denotes timepoint. (**C**) Median spatial distance (μm) from NK bins to the nearest bin of each cell type, per condition; warmer colors indicate closer proximity. (**D**) NK cell neighborhood proximity enrichment (observed/expected) for secreted and contact-dependent ligands at 60 days, comparing IRI (red) and sham (teal); arrows connect the sham and IRI value for each gene. Enrichment was assessed against a permuted spatial null. (**E**) Representative sections showing *Col4a1* expression density (green) with NK cell (red) and lymphatic cell (purple) bins overlaid on the H&E image.

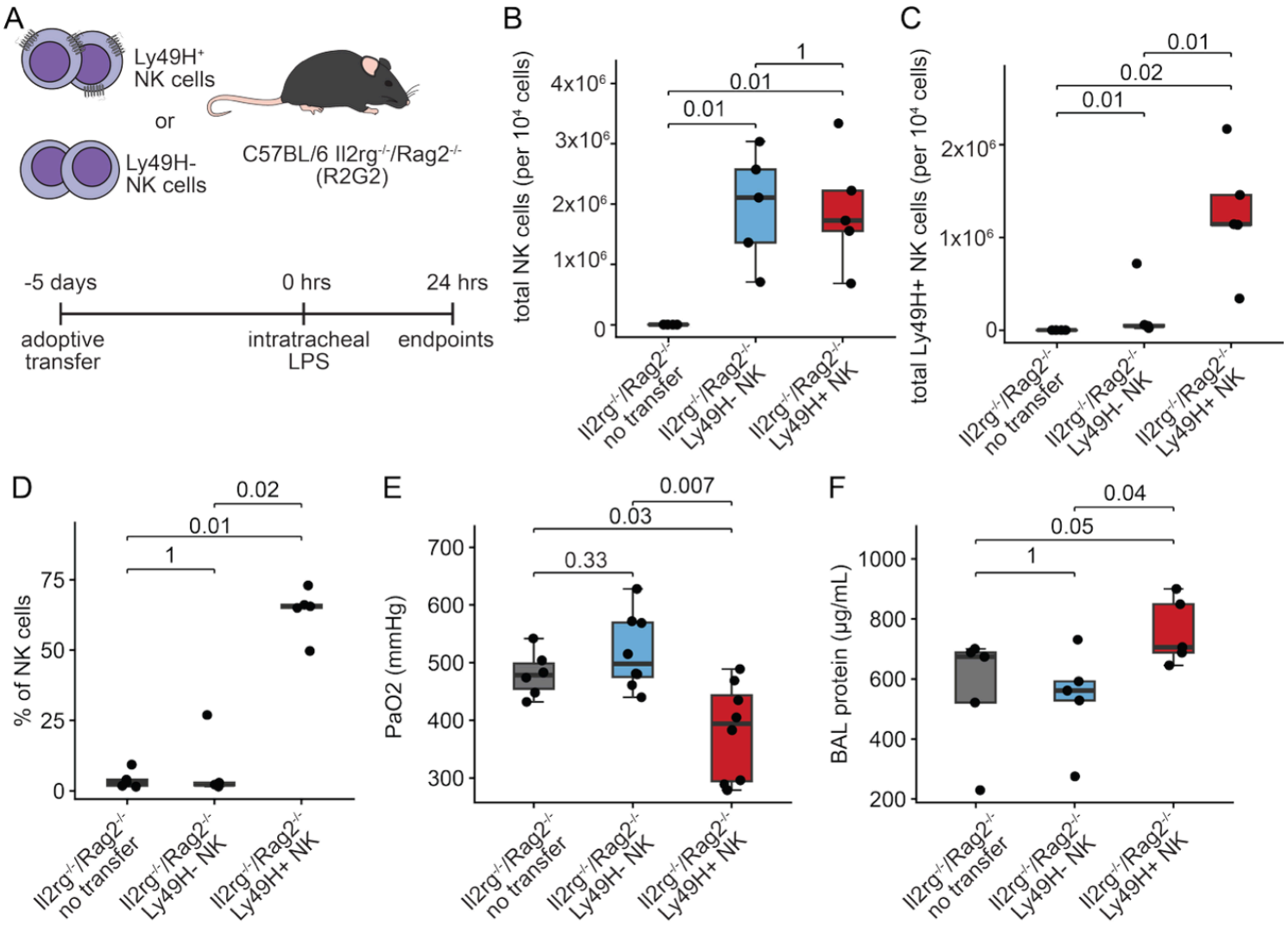


Figure 6

Adoptive transfer of CMV-experienced Ly49H⁺, but not Ly49H⁻, NK cells exacerbate acute lung injury. (**A**) Experimental schematic where Ly49H⁺ (n = 8) or Ly49H⁻ (n = 8) NK cells were sorted from latently

CMV infected donor mice and adoptively transferred into lymphocyte-deficient C57BL/6 *Il2rg*$^{-/-}$*Rag2*$^{-/-}$recipients on day −5. Acute lung injury was induced by intratracheal LPS. Control recipients (n = 6) received LPS without NK transfer. Reconstitution of the donor NK compartment was assessed by (**B**) total lung NK cells, (**C**) total lung Ly49H^{+} NK cells, and (**D**) Ly49H^{+} cells as a percentage of NK cells. Acute lung injury severity was measured by (**E**) Arterial oxygenation (PaO_2, mmHg) and (**F**) bronchoalveolar lavage (BAL) total protein (μg/mL). *P*-values are from two-sided pairwise Wilcoxon rank-sum tests.

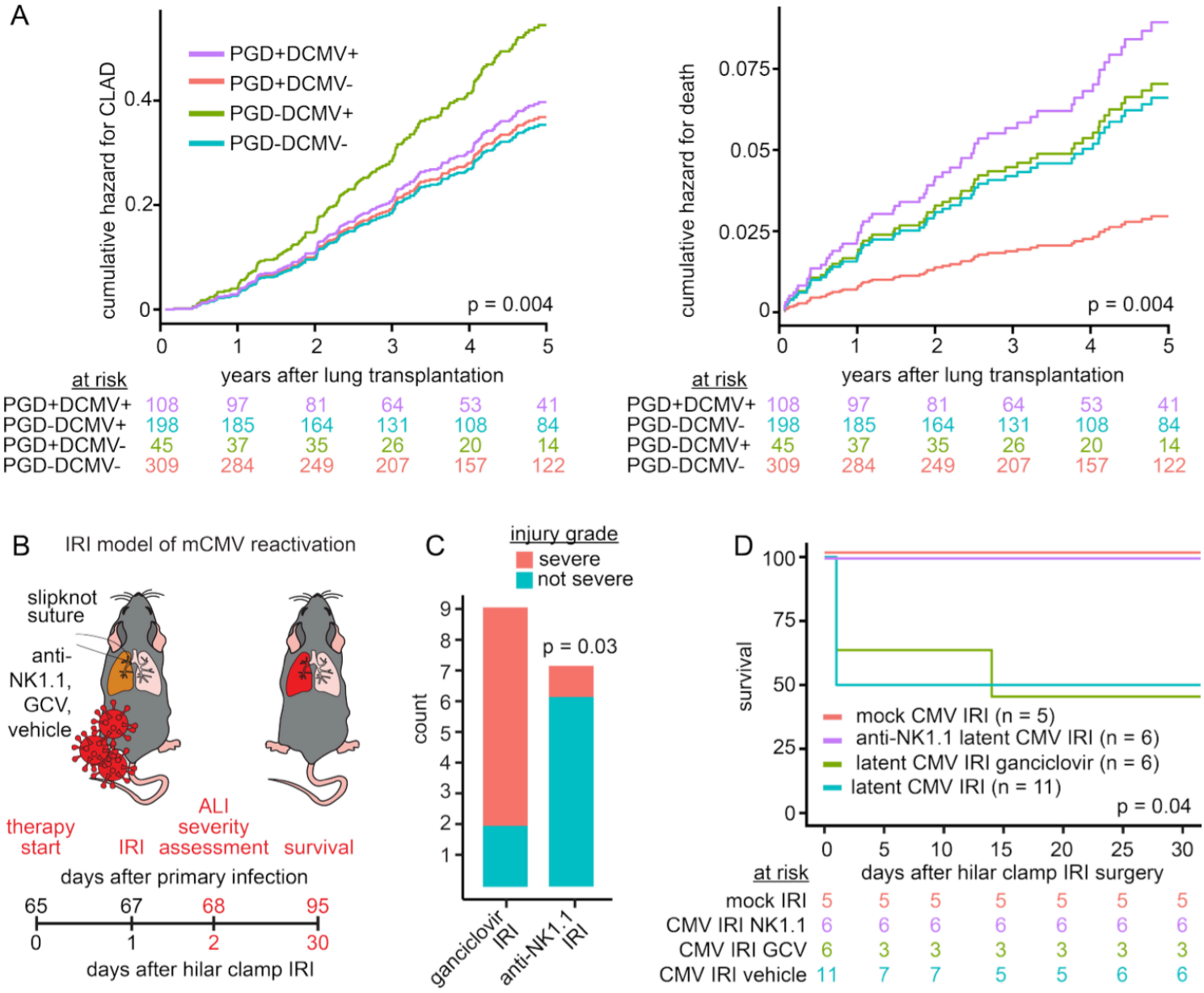


Figure 7

Human and mouse survival is worse in latent CMV and IRI. **(A)** Cumulative hazards for CLAD (left panel) and death (right panel) stratified by donor CMV serostatus and severe PGD are shown for a competing risk analysis in the clinical cohort, with risk tables displayed below each panel. (**B**) Schematic of the experimental mouse model of treatment with ganciclovir (GCV), anti-NK1.1 depletion, or vehicle

therapy preceding hilar clamp (HC) IRI procedures in mock or latent mCMV infected mice. Acute injury assessments were made at 1 day and survival was tracked through 30 days after IRI. **(C)** Latent CMV mice received ganciclovir (n = 9) or anti-NK1.1 (n = 7) 24 hours preceding HC. Bar plots are shaded for severe lung injury (PaO2<200 mmHg or death within 24 hours) versus not severe injury. **(D)** Kaplan-Meier survival curves across mouse experimental groups. Human survival data were analyzed using cause-specific Cox proportional hazards regression in a competing risks framework adjusted for age, sex, diagnosis, ethnicity, and transplant type. Differences in mouse injury severity were assayed with χ^2 testing and mouse survival was analyzed using the log-rank test with pairwise comparisons.

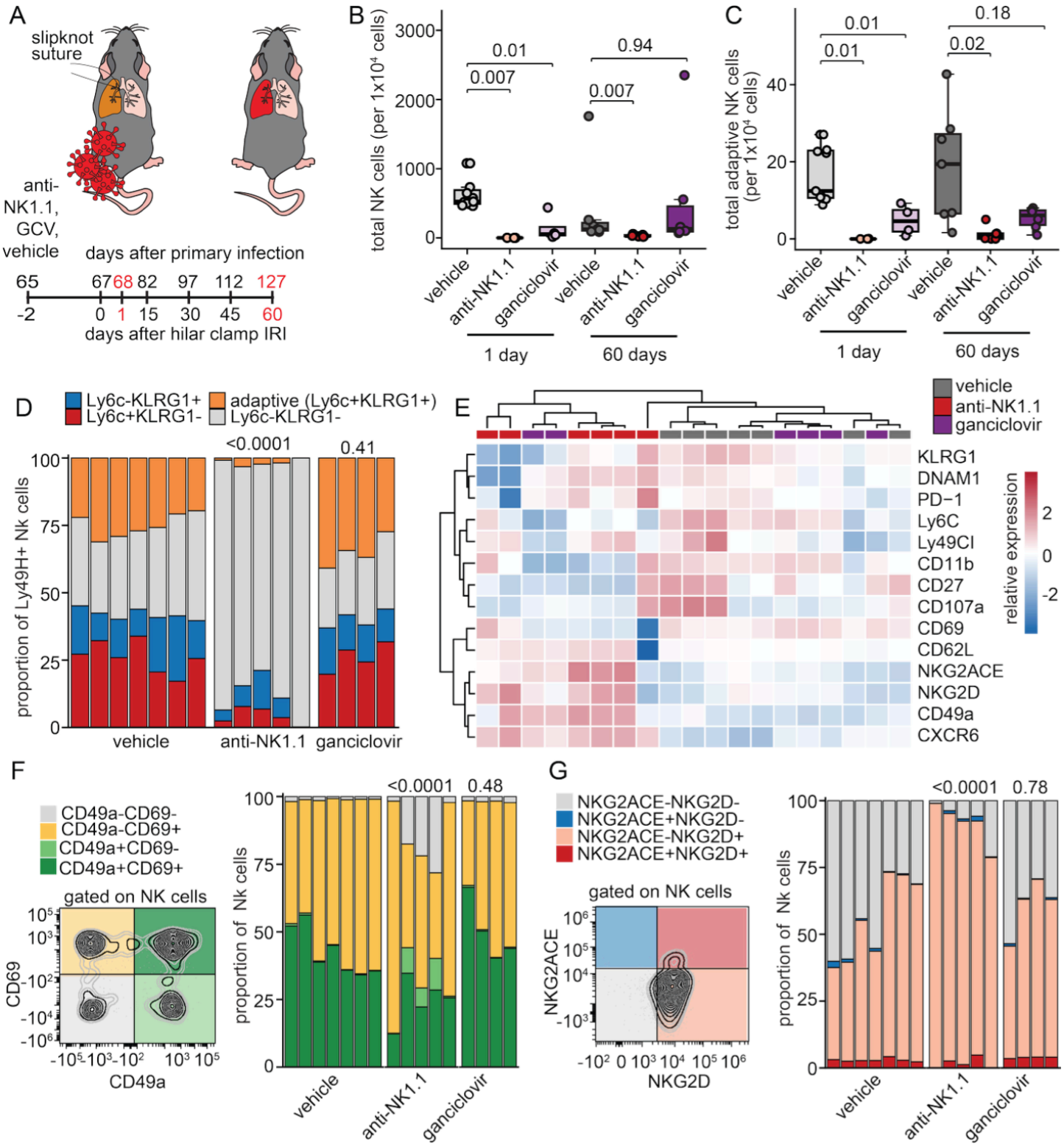


Figure 8

NK depletion resets the CMV-specific pulmonary niche. (A) Experimental schematic of latently mCMV-infected mice treated with anti-NK1.1 monoclonal antibody (NK depletion), ganciclovir (GCV) or vehicle control (vehicle) preceding hilar-clamp lung IRI. Lungs were procured at 1 and 60 days after IRI. **(B)** Total pulmonary NK cells by treatment at 1 and 60 days.

(C) Total adaptive NK cells by treatment group at 1 and 60 days. **(D)** Ly6c/KLRG1 subset composition of

NK cells at 60 days. **(E)** Heatmap of NK cell marker median fluorescence intensities clustered by sample and annotated by treatment type **(F)** NK cell tissue residency by CD49a and CD69 at 60 days. Representative contour plot (left) and per-sample quadrant composition (right). **(G)** NK cell NKG2ACE and NKG2D expression at 60 days. Representative contour plot (left) and per-sample composition (right). Box plots show median, interquartile range, and whiskers; each point is one mouse with at least n = 4 per condition. Continuous comparisons (**B, C**) used pairwise Wilcoxon tests with Benjamini-Hochberg adjustment; subset composition (**D, F, G**) was compared to vehicle by chi-square test, with the p value shown above each treatment group.

Supplementary Files

This is a list of supplementary files associated with this preprint. Click to download.

- SupplementalMaterial.docx